ONE DIMENSIONAL UNSTEADY MODEL OF A HYDROPNEUMATIC PISTON ACCUMULATOR BASED ON FINITE VOLUME METHOD

Filipp Kratschun*[1], Jens Köhne[2], Peter Kloft[2], Heiko Baum[3], Katharina Schmitz[1]

1: Institute for Fluid Power Drives and Systems ,RWTH Aachen University, Campus-Boulevard 30, 52074 Aachen
2: HYDAC Technology GmbH, 66280 Sulzbach/Saar
3: FLUIDON GmbH, Jülicher Straße 338a, 52070 Aachen
* Corresponding author: Tel.: +49 241 8047738; E-mail address: filipp.kratschun@ifas.rwth-aachen.de

ABSTRACT

Hydraulic piston accumulators play a major role especially within the field of stationary hydraulics. The calculation of the amount of hydraulic energy which can be stored in such an accumulator is crucial when it comes to a precise system design. The knowledge of the temperature and pressure within the accumulator is required in order to calculate the amount of energy to be stored. The state of the art solution to estimate the state of change of such an accumulator is the implementation of a costly measurement system within the accumulator which tracks the position of the piston.

The goal of this paper is to develop and to analyse a time efficient simulation approach for the gaseous phase within a piston accumulator depending on the accumulator's load cycle. Temperature, pressure, density and velocity profiles inside of the gaseous phase are calculated transiently in order to achieve that goal. The simulation model is derived in one dimensional environment to save computational effort. Having derived a valid model of the gaseous phase it will be possible in future works to replace the expensive position measurement system by pressure and temperature transducers and then use the model to calculate the position of the piston and therefore estimate the state of change.

Keywords: Hydraulic Accumulator, Gas Spring, Change of State, Finite Volume, Gas Dynamics

1. INTRODUCTION

In many fields of engineering hydraulic accumulators play a crucial role. Their possibility to absorb and deliver high peak loads within a very short period of time and the robust design make them indispensable in the field of aircraft engineering, renewable energies, mobile and stationary machinery. A hydro-pneumatic piston accumulator consists of a gaseous volume filled with nitrogen and separated from the hydraulic fluid by a piston.

A dynamic pressure increase within the system resulting from an instant peak load leads to a compression of the nitrogen's volume. In other words the energy of the dynamic load is stored in form of compression energy within the accumulator. The amount of stored energy in the accumulator depends on the change of state during the compression of the nitrogen. For high pressure gradients the change of state is assumed to be isentropic whereas for low gradients the change of state is assumed to be isothermal.

In real applications the change of state is in between of isothermal and isentropic and therefore unknown. This makes it impossible to calculate the exact amount of energy which can be stored or released by the accumulator for a given system for arbitrary dynamic processes. Consequently, the design of a system including a hydraulic accumulator is always connected with inaccuracy. Commonly used methods to estimate the change of state in a hydraulic accumulator make use of the polytropic exponent [1] or the eigen frequency [2], [3]. Both methods rely on measurements of the given geometry and have to be carried out close to the operating conditions of the given device to be designed. This implies tremendous costs and time for the design of the perfect fitting accumulator for a given system. Another method presented by [4] calculates the temperature directly but only for small changes in pressure.

In order to overcome these difficulties this paper presents a simulation modeling approach of a hydraulic accumulator in order to calculate the

temperature and, therefore, the change of state inside of it without measurements for arbitrary operating conditions. The developed model implies the heat transfer between the gaseous phase and the surrounding boundaries.

The working principle of a hydro-pneumatic piston accumulator is depicted in **Figure 1.** The hydraulic oil delivered by the system compresses the nitrogen stored inside the accumulator. The compression energy W_P leads to an increase in the nitrogen's temperature.

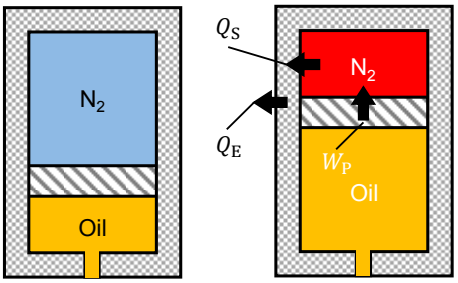

Figure 1: Working principle and energy balance for pistion accumulator

The temperature increase leads to a heat flux from the nitrogen into the surrounding body Q_S which therefore increases its temperature leading to a further heat flux Q_E between the surrounding body and the environment. The amount of the stored energy strongly depends on the temperature inside the nitrogen phase.

The possible scenarios are depicted in **Figure 2.** It is assumed that for a very slow compression the the temperature remains unchanged, whereas for a very quick compression the temperature is calculated using the isentropic phase change. All the changes in between are described by a polytropic exponent. Using the compression ratio ϵ given by (1) the pressure can be calculated using (2).

$$\epsilon = \frac{v_1}{v_2} \tag{1}$$

$$p_2 = p_1 \epsilon^n \tag{2}$$

Two problems arise if this method is used to predict the pressure and therefore the amount of energy to be stored in the given accumulator.

1. The polytropic exponent is dependent on the geometry and the compression velocities, but there is no way yet to quantify it depending on these values.
2. This paper reveals that the upper threshold of $n = \kappa$ is not valid. The polytropic exponent for a compression within a hydraulic accumulator can reach arbitrary values above κ.

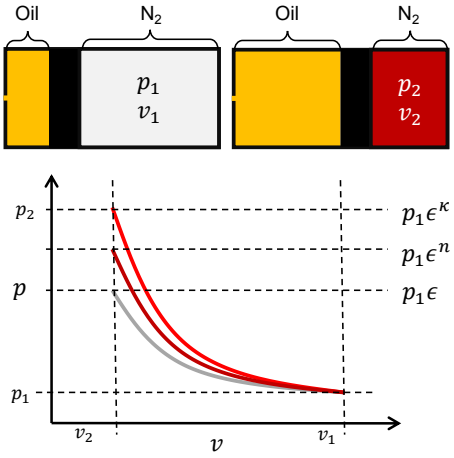

Figure 2: Change of state within a hydraulic piston accumulator

To overcome both problems pressure, temperature, and velocities have to be resolved within the nitrogen phase during the compression. The heat fluxes between the nitrogen and the boundaries have to be calculated depending on the position inside the gaseous phase.

The paper is structured as follows: In the second section the pressure, temperature, density and velocity profiles are calculated adiabatically and without dissipation. In the third part heat transfer and dissipation are added to the calculation. In the fourth section the developed model is validated using a test rig. A brief conclusion is given in the final section.

2. ADIABATIC CALCULATION OF THE GAS

In order to calculate the temperature, pressure, density and velocity profiles in the gaseous phase during a compression or an expansion Eulerian equations given in (3) have to be solved along the gaseous phase length. The vector form of (3) is depicted given by (4), see [5].

$$\begin{pmatrix} \rho \\ \rho u \\ E \end{pmatrix}_t + \begin{pmatrix} \rho u \\ \rho u^2 + p \\ u(E+p) \end{pmatrix}_x = \begin{pmatrix} 0 \\ 0 \\ 0 \end{pmatrix} \tag{3}$$

$$U_t + F(U)_x = 0 \tag{4}$$

Since the compression or expansion process is arbitrary dynamic and there is no exact solution for (4) a finite volume approach is chosen which is presented in **Figure 3**.

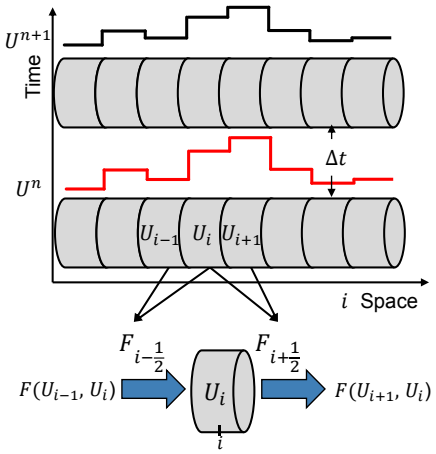

Figure 3: Finite volume method for the inner part of the accumulator

The gaseous phase is discretized in x-direction. In order to calculate the change of mass, momentum or energy within the volume Δx during a time step Δt, it is necessary to construct numerical fluxes $F_{i\pm\frac{1}{2}}$ at the volume's borders. This is done here applying the flux vector splitting solver presented by Steger and Warming [6] given by (5), (6) and (7). This approach calculates positive and negative parts of an inter cell flux with respect to the eigen velocities λ_i of the system. These velocities represent the speed of information propagation inside each cell and are given by (8).

$$F_{i+\frac{1}{2}} = F_i^+ + F_{i+1}^- \tag{5}$$

$$F_i^\pm = \frac{\rho}{2\kappa}\begin{pmatrix} \lambda_1^\pm + 2(\kappa-1)\lambda_2^\pm + \lambda_3^\pm \\ (u-a)\lambda_1^\pm + 2(\kappa-1)u\lambda_2^\pm + (u+a)\lambda_3^\pm \\ (V-ua)\lambda_1^\pm + 2(\kappa-1)u^2\lambda_2^\pm + (V+ua)\lambda_3^\pm \end{pmatrix} \tag{6}$$

$$V = \frac{1}{2}u^2 + \frac{a^2}{\kappa-1} \tag{7}$$

$$\lambda_1 = u-a,\ \lambda_2 = u,\ \lambda_3 = u+a \tag{8}$$

Herein, u is the flow velocity and a the speed of sound which is given by (10), wherein R is the specific gas constant. The sign of the eigenvalues $\lambda_{1,2,3}^\pm$ can be determined using (9) and therefore, the flux given by (6) can be determined for each cell.

$$\lambda_{1,2,3}^\pm = \lambda_{1,2,3} \pm |\lambda_{1,2,3}| \tag{9}$$

$$a_i = \sqrt{\kappa R T_i} \tag{10}$$

The calculation of the flux is estimated and the numerical scheme for each cell of the gaseous phase is finally given by (11).

$$U_i^{n+1} = U_i^n + \frac{\Delta t}{\Delta x}\left(F_{i-\frac{1}{2}} - F_{i+\frac{1}{2}}\right) \tag{11}$$

Thus, calculation of the inner part of the discretized gaseous domain is known now. To enable a compression the boundaries of the numerical domain have to be treated in a different way compared to (5) to find a correct flux formulation.

Fortunately, it is possible to solve the Eulerian equations analytically at the border of a moving wall and one cell exactly. If the wall moves with a lower velocity than the velocity of the first cell ($u_\mathrm{w} < u_1$), an expansion wave is formed whose pressure p_w at the wall can be calculated by (12).

$$p_\mathrm{w} = p_1\left(1 - \frac{\kappa-1}{2}\frac{u_1 - u_\mathrm{w}}{a}\right)^{\frac{2\kappa}{\kappa-1}} \tag{12}$$

For the case of the wall velocity being greater than the velocity of the first cell ($u_\mathrm{w} > u_1$), a shock wave is formed, and the pressure at the wall p can be expressed via (13) [7].

$$p_w = p_1\left(1 + \left(\frac{u_1+u_w}{2C^2}\right)^2 + \frac{u_1+u_w}{2C^2}\sqrt{\frac{8\kappa}{\kappa-1}C^2 + (u_1+u_w)^2}\right) \tag{13}$$
$$C = \frac{2p_1}{(\kappa+1)\rho_1}$$

Since pressure and velocity at the wall are calculated analytically, the flux of the moving wall is fully defined and is presented in (14).

$$F_\mathrm{w} = \begin{pmatrix} 0 \\ p_\mathrm{w} \\ u_\mathrm{w} p_\mathrm{w} \end{pmatrix} \tag{14}$$

In front of the moving piston the first cell's volume can be arbitrary small immediately resulting in solver instabilities. To solve this problem the cut cell approach presented by [7] is applied. It is sketched in **Figure 4**.

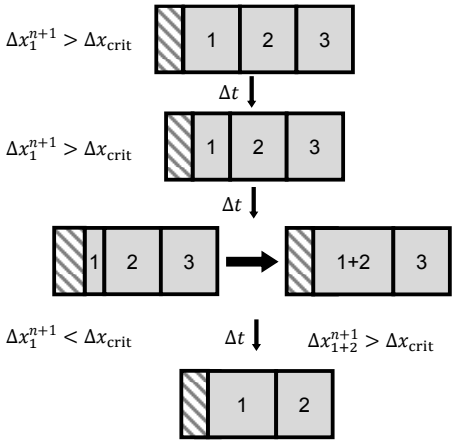

Figure 4: Cut cell approach

The basic idea behind this approach is to merge the first cell in front of the piston with the second cell when the first cell undercuts a critical volume Δx_{crit}. To understand the merging approach, first of all one has to clarify, that the volume of the first cell is not constant and varies in time, see (15).

$$\Delta x_1^{n+1} = \Delta x_1^n - u_{\mathrm{w}}^n \Delta t \qquad (15)$$

Bearing in mind that the entire calculation is carried out using conservative variables, conversion of mass, momentum and energy lead to the trivial equation for the first cell, when its volume is changed (16).

$$U_1^{n+1} = U_1^n \frac{\Delta x_1^n}{\Delta x_1^{n+1}} \qquad (16)$$

It simply states, that the change of volume of a cell does not result in a change of the conservative quantity, for instance, if the volume is reduced due to a compression, the ratio $\frac{\Delta x_1^n}{\Delta x_1^{n+1}}$ becomes greater than unity and the density would increase.

When merging is applied the new cell's volume Δx_1^{n+1} is simply the sum of the first and second cell $\Delta x_1^n + \Delta x$ before merging is executed. The new conservative values of the new first cell are then simply given by (17) to maintain mass, momentum and energy annihilation.

$$\Delta x^n = \Delta x + \Delta x^n, \qquad U_1^n = \frac{U_1^n \Delta x_1^n + U_2^n \Delta x}{\Delta x_1^n + \Delta x} \qquad (17)$$

Due to the merging the volume of the first cell is now much greater compared to the critical volume and (17) can be used in order to calculate the first cell's value. If the first cell is expanded, it has to be divided once its value exceeds the threshold of $\Delta x^n = \Delta x + \Delta x_{\mathrm{crit}}$. The values of the two new cells are simply the value of the cell before division and won't be threated here. The resulting numerical scheme for the first cell is then given by (18).

$$U_1^{n+1} = U_1^n \frac{\Delta x_1^n}{\Delta x_1^{n+1}} + \frac{\Delta t}{\Delta x_1^{n+1}} \left(F_{\frac{3}{2}} - F_{\mathrm{w}} \right) \qquad (18)$$

The embodiment of this approach enables the calculation of compression and expansion within a finite volume approach using conservative variables. In other words, the pressure, temperature, density and temperature profile in the gaseous phase can be calculated during a compression or expansion without heat exchange and dissipative effects. The simulation routine was implemented in DSHplus® software.

To validate the derived method modal acoustic theory is applied [8] [9]. Invoking a pipe with closed endings filled with air and one ending being excited i.e. moving back and forth with a low amplitude one can calculate the frequencies which induce resonance patterns using (19).

$$f_n = \frac{k}{2} \frac{a}{L} \qquad (19)$$

Herein, k is the resonance order, a the speed of sound and L the total length of the pipe.
Figure 5 depicts the pattern for the first and second resonance frequencies.

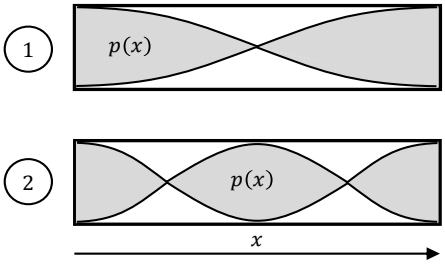

Figure 5: Closed endings resonance pattern

The pressure distribution for the resonance case always consists of one more antinodes than nodes and the antinodes are always at the borders of the pipe. To validate the procedure presented above a pipe of the length $L = 1\,m$, an initial temperature of $T = 290\,K$ resulting in a speed of sound of $a = 341 \frac{m}{s}$ is excited with small amplitude $\hat{x} = 0.1\,mm$ and a frequency of 50 Hz

to 750 Hz. The initial pressure of the pipe is 10 bar. Applying (19) the first four resonance frequencies given by **Table 1** lie within this range and if the simulation routine is correct the resonance patterns described above should occur at exactly these frequencies.

Table 1: Closed ending resonance frequencies

Order	1	2	3	4
Frequency[Hz]	171	342	513	684

Figure 6 presents the frequency dependent pressure deviation distribution $\bar{p} = \frac{p}{p_{\text{initial}}}$ by applying the simulation routine described above.

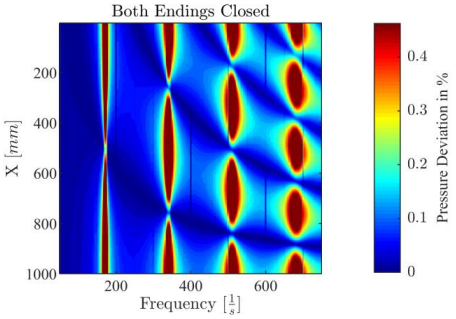

Figure 6: Resonance pattern for both endings closed

One can clearly see that the resonance patterns occur exactly at the frequencies predicted by the theory. Moreover, the sequence of nodes and antinodes is also exact.

For further validation of the presented approach the polytropic exponent for a simulated compression is sought (20). Herein, p_2 is the mean dynamic pressure within the nitrogen phase at the end of the compression (21) and p_1 is the pressure in the nitrogen phase at the beginning of the compression and L the length of the gas phase.

$$n = \frac{\ln\left(\frac{p_2}{p_1}\right)}{\ln(\epsilon)} \tag{20}$$

$$p_2 = \frac{1}{L}\sum_{i=1}^{M}\left(\frac{\Delta x_i p_i}{\kappa - 1} + \frac{\rho_i}{2}\left(u_i^2\right)\right)(\kappa - 1) \tag{21}$$

The results for an adiabatic compression ratio of $\epsilon = 1.25$ depending on the piston's velocity are presented in the **Figure 7**.

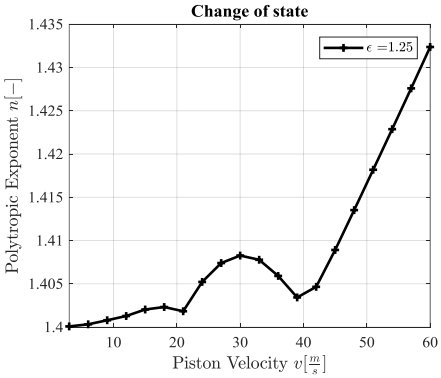

Figure 7: Change of state for a compression

It is remarkable that in contradiction to the theory the polytropic exponent exceeds the value of κ which is in this case 1.4. An increasing piston velocity or in other words a higher compression speed leads to increasing values of n. Furthermore, there is a local maximum at $30\frac{m}{s}$. To seek for the answer to the possible contradiction to theory one has to invoke the very derivation of mechanical work done to the system in conjunction with the theory of a polytropic phase change [10]. **Figure 8** shows an incremental compression of a gas spring and its mathematical formulation given by (22).

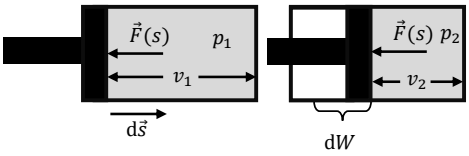

Figure 8: Work delivered to a gas spring

The gas pressure applies a force on the piston which is proportional to the piston's area. So, the incremental compression $d\vec{s}$ and the force $\vec{F}(s)$ can be expressed using volume and pressure instead of force and distance resulting in the integrated form (23).

$$dW = \vec{F}(s) \cdot d\vec{s} = -pA\frac{dV}{A} \tag{22}$$

$$W_{1,2} = -\int_{v_1}^{v_2} p(v)\, dv \tag{23}$$

For the function $p(v)$ a polytropic approach is chosen which leads to (24) or (25) for $n = 1$.

$$W_{1,2} = \frac{v_1 p_1}{n-1}(\epsilon^{n-1} - 1) \quad (24)$$

$$W_{1,2} = v_1 p_1 \ln(\epsilon) \quad (25)$$

The polytropic approach implies that the pressure within the gas is uniform during compression. This means that the pressure before the piston is the same as the pressure in the rest of the vessel. In fact, the pressure in front of the piston cannot be the same as the pressure far away from it, because the speed of sound of the medium has a finite value. A closer look inside the gas phase of the accumulator during compression for different piston velocities shows this behaviour, see **Figure 8** - **Figure 11** [10]. In these graphs the pressure distribution of the normalised pressure $\frac{p}{p_{\text{initial}}}$ are plotted against the vessel's length for 25%, 50% 75% and 100% of the compression time elapsed.

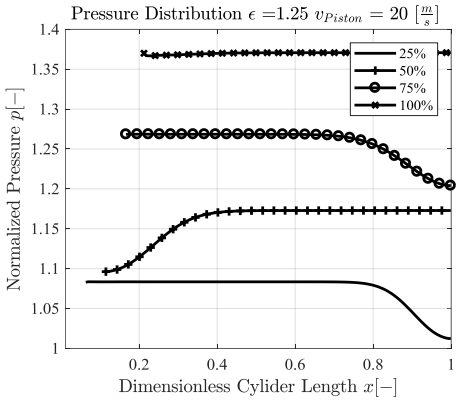

Figure 8: Pressure distribution for different stages of the compression at $v_{Piston} = 20\frac{m}{s}$

The initiation of the compression creates a pressure wave that travels from left to right and is reflected by the rigid wall on the right side and the moving piston on the left side. The amplitude and speed of the compression wave depend on the speed of the piston and the temperature of the gas. A higher pressure compared to the average pressure at the piston and a higher speed inevitably lead to a higher energy demand to fulfil the compression, resolving the above mentioned contradiction. Therefore the polytropic exponent must increase with increasing piston speed..

At a piston speed of 20 m/s, the pressure wave passes through the vessel exactly four times. Each time the pressure wave travels from left to right, the piston must work against a relatively high pressure, while the piston must work against a relatively low pressure compared to the medium pressure when the wave is reflected at the wall. For the case of 30 m/s, the pressure wave has run back and forth once and has been reflected once by the piston. This means that the piston has to work against a relatively high pressure more often than against a relatively low pressure. This leads to a higher amount of energy required for compression and explains the relative maximum of the polytropic exponent at 30 m/s.

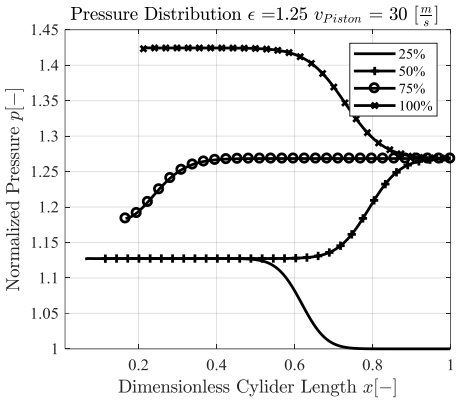

Figure 9: Pressure distribution for different stages of the compression at $v_{Piston} = 30\frac{m}{s}$

At a piston speed of 40 m/s, the pressure wave runs back and forth exactly once, resulting in a relatively low compression energy compared to 30 m/s.

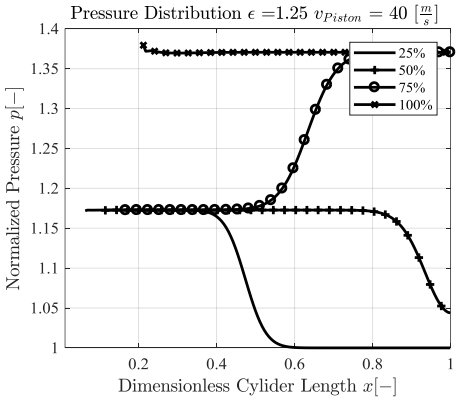

Figure 10: Pressure distribution for different stages of the compression at $v_{Piston} = 40\frac{m}{s}$

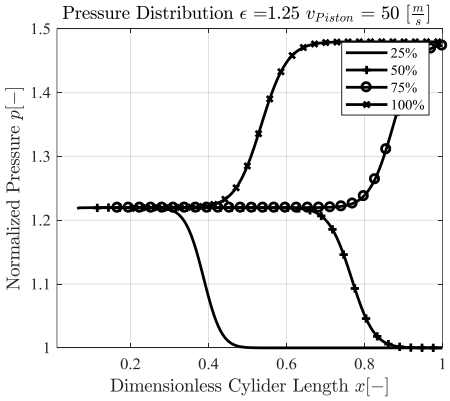

Figure 11: pressure distribution for different stages of the compression at $v_{Piston} = 50\frac{m}{s}$

For a piston velocity of $50\frac{m}{s}$ 65% of the compression takes place at a relatively high pressure resulting in a higher amount of compression work compared to $40\frac{m}{s}$. For increasing piston velocities above $50\frac{m}{s}$ the compression takes place at relatively high pressures only. This results in a higher amount of compression energy needed. **Figure 12** depicts the mean pressure of the first cell at the piston during the compression in relation to the mean pressure of the entire vessel. The shape of the graph is exactly the same as of the polytropic exponent given in figure 5, which proves the validity of the explanations given above.

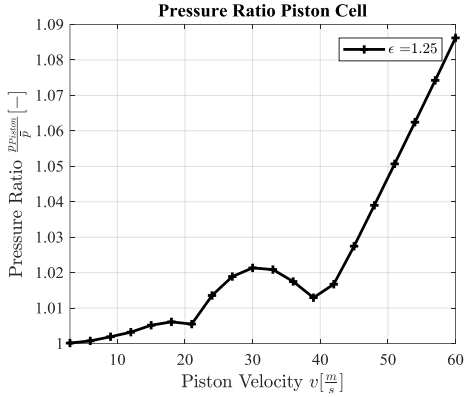

Figure 12: Pressure ratio of the first cell to the mean pressure

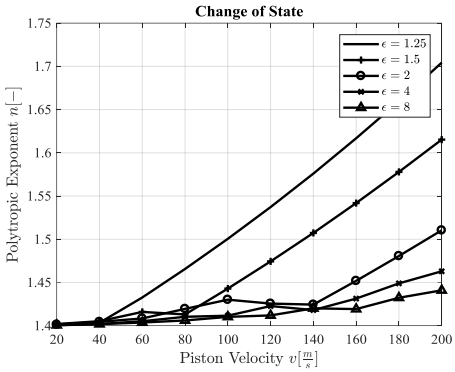

Figure 13: Change of state for different compression ratios

Finally, the polytropic exponents depending on the piston velocity and the compression ratio are calculated and presented in **Figure 13**. The results reveal that for a higher compression ratio the change of state becomes more and more isentropic. The reason for this is that for higher compressions the mean pressure during the compression is higher. Therefore, the amplitude of the pressure waves compared to the mean pressure is smaller. This results in a smaller deviation from the theory of a uniform pressure distribution and consequently in a smaller deviation from the theory which states that the change in state of an adiabatic vessel has to be isentropic, i.e. $n = 1.4$. Moreover, it proves that the implemented simulation represents the physics correctly.

3. DIABATIC CALCULATION OF THE GAS PHASE

The previous results were based upon the assumption of an ideal flow neglecting heat transfer and dissipation. In order to incorporate these effects into the simulation the Eulerian equations have to be updated from (3) to (26).

$$\begin{pmatrix}\rho\\ \rho u\\ E\end{pmatrix}_t + \begin{pmatrix}\rho v\\ \rho u^2 + p\\ u(E+p)\end{pmatrix}_x = \begin{pmatrix}0\\ -\frac{1}{2D}\lambda_f \rho u|u|\\ \frac{1}{2D}\lambda_f \rho u^2|u| - \frac{4\alpha(T-T_a)}{D}\end{pmatrix} \quad (26)$$

The new system of equations includes the shear stress at the vessels wall using the friction coefficient λ_f in the momentum equation and the resulting dissipation in the energy equation of (26). Herein, Re_i is the Reynolds number of each finite volume for either laminar or turbulent flow regime.

$$\lambda_f = \frac{64}{Re_i}, \qquad \lambda_f = \frac{0.3164}{\sqrt[4]{Re_i}} \tag{27}$$

The heat transfer between the fluid and the wall is included using the heat transmission coefficient α. The estimation of the heat coefficient is sought using the Nusselt number given by (28), wherein λ_h is the heat conductivity of the nitrogen and D the inner diameter of the vessel.

$$Nu_D = \frac{\alpha D}{\lambda_h} \tag{28}$$

The Nusselt number is calculated invoking the Reynolds Analogy [11] given in (29). This assumption is valid for Prandtl Numbers near unity, because for this case the thickness of the temperature boundary layer is of the same order as the thickness of the velocity boundary layer. In other words, the gradient of the temperature i.e. the heat flux can be expressed via the gradient of the velocity, i.e. the shear stress at the wall.

$$Nu_D = \frac{1}{8} Re \lambda_f \tag{29}$$

For diminishing flow velocities Nu_D is assumed to be 3, see [4]. Numerically, the right hand side of (26) is simply added to the scheme resulting in a source term which can for example be treated using a fractioning time step method [5].

Figure 14 depicts the results for a simulated compression including heat transfer and dissipation for a ratio of $L/D = 100$.

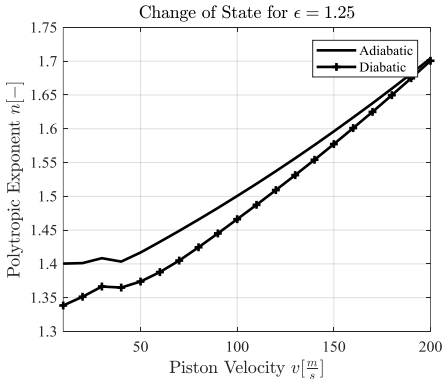

Figure 14: Comparision of diabatic and adiabatic change of state

As expected, the polytropic exponent is reduced by the heat escaping from the accumulator. Nevertheless, the shape of the curve with a local maximum at 30 m/s remains the same as in the adiabatic case, see **Figure 15.** Furthermore, as expected, the polytropic exponent tends towards the values of an adiabatic change of state with increasing piston speeds, since the time for heat transfer decreases with increasing piston speed. This leads to less heat transfer.

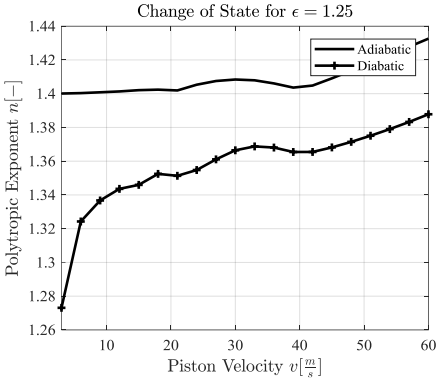

Figure 15: Comparision of diabatic and adiabatic change of state

As there is no analytical case to validate the diabatic results, the validation is carried out with a test rig, which is described in the following chapter.

4. EXPERIMENTAL VALIDATION

In order to validate the simulation method experimentally, a test rig including a piston accumulator with an inner diameter of $D = 0.18\ m$ and a length $L = 1.01\ m$ of the gas phase is set up. The accumulator is equipped with a measurement system of the piston's position inside the gas phase. The pressure within the gas is tracked with a transducer and the initial temperature is measured at the closed ending. The accumulator is filled with nitrogen and to maintain the validity of the ideal gas equation the highest pressure of the experiments does not exceed 25 bar. The set up is depicted in **Figure 16.**

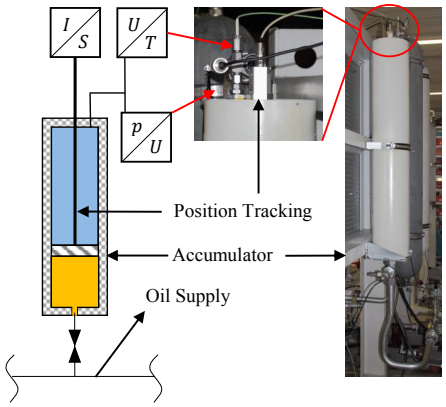

Figure 16: Test rig set up

The experimental procedure is as follows: The accumulator is filled quickly with oil which leads to a fast compression of the nitrogen of up to $\epsilon = 5$. Then the accumulator is discharged slowly. The tracked piston's position is included into the simulation procedure as input leading to a compression or expansion of the gas phase. The pressure is calculated applying the presented model and compared to the measured pressure.

Figure 17 presents the results of the measurement. Especially for the compression the deviation of measurement and simulation is negligible proving the simulation procedure to be valid. Yet, between 8 s and 20 s there is a deviation between the measured and simulated values. The simulated pressure is higher compared to the experimental results. This is closely connected to the temperature of the measured and simulated system. For the simulated case the temperature and therefore, the pressure is higher compared to the measured case for two reasons.

Firstly, within the real system natural convection occurs, especially for the case of diminishing piston velocities this comes into play and explains the deviation starting at approximately 10 s. Secondly, the position measurement system is connected to the piston in the gas phase mechanically. The mechanical construction reaching inside the gas is responsible for direct heat conduction from inside the gas phase to the outer boundaries of the accumulator accelerating the heat transmission outside the gas phase. Both effects described above force a quicker cooling of the gas and therefore a lower pressure.

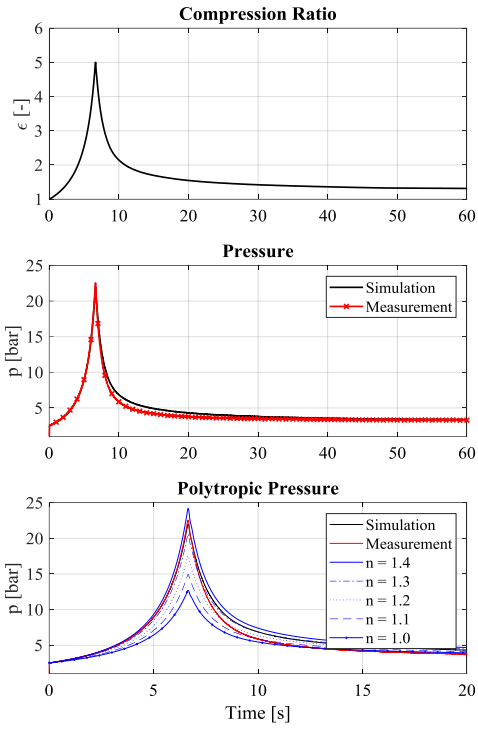

Figure 17: Simulation vs. experimental results

Comparing the simulation results with the polytropic approach (**Figure 17)** between 2.5 s and 12 s the measured pressure crosses all polytropic curves. It reveals the inherent weakness of this approach, since it is impossible to assign "one" polytropic exponent for the process. It displays the advantage of the derived approach including a discretization of the inner part of the accumulator.

5. CONCLUSION AND OUTLOOK

The paper presents a novel approach to calculate the pressure inside a hydro-pneumatic accumulator based on the compression rate. The method is validated analytically and experimentally. The results reveal a very good agreement between simulation and measurement especially taking into account the uncertainties connected to the experimental set up. Yet, there is room for improvement, especially for diminishing piston velocities the model's accuracy has to be increased. The huge advantage of the presented approach is its usability since no parameterization including measured values like

heat transfer coefficients or eigen frequencies [2] are needed. Its gas dynamics computational core allows arbitrary compression ratios and velocities.

NOMENCLATURE

α	heat transfer coefficient
ϵ	compression ratio
λ	eigenvalue
λ_f	coefficient of friction
λ_h	heat conductivity of the gas
κ	isentropic exponent
ρ	density
a	speed of sound
D	diameter
L	length of the gas phase
M	total amount of finite volumes
Nu	Nusselt Number
p	pressure
U	conservative variable
v	particle velocity

REFERENCES

[1] Schmitz,K., Murrenhoff, H. ”Fundamentals of Fluid Power. Part 1: Hydraulics”, Shaker Verlag, 2018

[2] Rupprecht, K., R. “Hydrospeicher – experimentelle und analytische Untersuchung zur Energiespeicherung”, Ph.D. Thesis, Aachen, 1988

[3] Rotthäuser, S., “Verfahren zur Berechnung und Untersuchung hydropneumatischer Speicher”, Ph.D. Thesis, Aachen, 1993

[4] Pelz, P., Buttenbender, J., “The dynamic stiffness of an air-spring”, ISMA2004, Leuven, 2004

[5] Toro, E. F., ”Riemann Solvers and Numerical Methods for Fluid Dynamics”, Springer Verlag, 2009

[6] Steger, J. L., Warming, F. R., “Flux Vector Splitting of the Inviscid Gasdynamic Equations with Application to Finite-Difference Methods”, Journal of Computational Physics 40 (263-293), 1981

[7] G. Yang et al., “A cartesian cut cell method for compressible flows Part B: moving body problems”, The Aeronautical Journal, 1997

[8] Nieter, J.J., Singh, R., “Acoustic modal analysis experiment”, Journal of the Acoustical Society of America, Vol. 72, 1982

[9] Sinambari, Gh., R., Sentpali, S., “Ingenieurakustik” , Springer Verlag, 5. Auflage, 2014

[10] Kratschun, F., Rambaks, A., Schmitz, K.: ”Fully Transient Model of a Hydraulic Accumulator”, Conference Proceedings, International Mechanical Engineering Congress and Exposition, Salt Lake City, Utah, United States of America, 2019

[11] Schlichting, H., Gersten, K., “Grenzschichttheorie”, Springer Verlag, 10. Auflage, 2006